IEEE Access
Multidisciplinary ⋮ Rapid Review ⋮ Open Access Journal

Received 6 August 2023, accepted 6 September 2023, date of publication 11 September 2023,
date of current version 20 September 2023.

Digital Object Identifier 10.1109/ACCESS.2023.3313724

RESEARCH ARTICLE

Design of a Metal 3D Printed Double-Ridged Horn Antenna With Stable Gain and Symmetric Radiation Pattern Over a Wide Frequency Range

NAMKANG LEE[1], CHANGHYEON IM[1], SEULGI PARK[2], AND HOSUNG CHOO[1], (Senior Member, IEEE)
[1]Department of Electronic and Electrical Engineering, Hongik University, Seoul 04066, South Korea
[2]Hanwha Systems Company Ltd., Seongnam 04541, South Korea

Corresponding author: Hosung Choo (hschoo@hongik.ac.kr)

This work was supported by the Hanwha Systems.

ABSTRACT In this paper, we propose a metal 3D printed double-ridged horn antenna with a truncated cone feeding structure, curve-shaped cavity, and mode suppressor for a feeder of a reflector antenna. The truncated cone feeding structure is employed to obtain symmetrical patterns, and the curve-shaped cavity is implemented to obtain broadband characteristics. The mode suppressor is then applied to maintain a stable bore-sight gain. To simplify the manufacturing and assembly process, the proposed antenna is designed with only two parts and is fabricated using metal 3D printing technology. To verify the performance of the antenna, the voltage standing wave ratio (VSWR), bore-sight gains, and radiation patterns are measured in a full anechoic chamber. The measured VSWR shows a maximum of 3.0 and an average of 1.9 from 2 GHz to 18 GHz. At 2 GHz, the measured bore-sight gains in the radiation pattern are 5.37 dBi for co-polarization and −20.7 dBi for cross-polarization. The measured radiation patterns are in good agreement with the simulated results.

INDEX TERMS Double-ridged horn, reflector antenna feeder, broadband antenna, 3D printing.

I. INTRODUCTION

In recent years, there has been growing use of Signal Intelligence (SIGINT) satellites to collect various electronic signals from neighboring countries for protection against potential threats. These satellites accumulate signals from several application fields, such as mobile satellite communications (S-band), synthetic aperture radar (C-band), military radar (X-band), and satellite broadcasting (Ku-band) [1], [2], [3], [4], [5]. As each application uses different frequency bands, payload antennas for SIGINT satellites are required to have broadband characteristics. These antennas are then desired to have stable high-gain performance, which enables them to effectively receive signals that are extremely weak due to high path loss. The preferred solution satisfying these requirements is a large-aperture reflector antenna with a feeder at the focal position [6], [7]. In such a reflector antenna, the feeder is the critical component for receiving signals, while the reflector serves to focus the signals onto the feeder. For example, when the feeder does not have the required symmetrical pattern, the spillover and illumination efficiencies may decrease, resulting in overall antenna performance degradation. Therefore, it is important to design a suitable feeder for the SIGINT satellite's reflector antenna, which requires broadband characteristics, stable high-gain performance, and symmetrical radiation patterns [8], [9]. Extensive research on feeders has been conducted while employing various antenna types such as patch arrays, log-periodic dipole arrays (LPDAs), and horn antennas [10], [11], [12]. Although patch antennas can easily obtain stable gain, they have limited potential to achieve broadband characteristics. In contrast, LPDAs typically exhibit broadband characteristics, but it is difficult to attain stable gain in a wide bandwidth [13]. Compared to the above two types of antennas, the horn antenna usually has broadband characteristics since it uses a waveguide port, and it has stable gain by a relatively large open

The associate editor coordinating the review of this manuscript and approving it for publication was Pavlos I. Lazaridis.

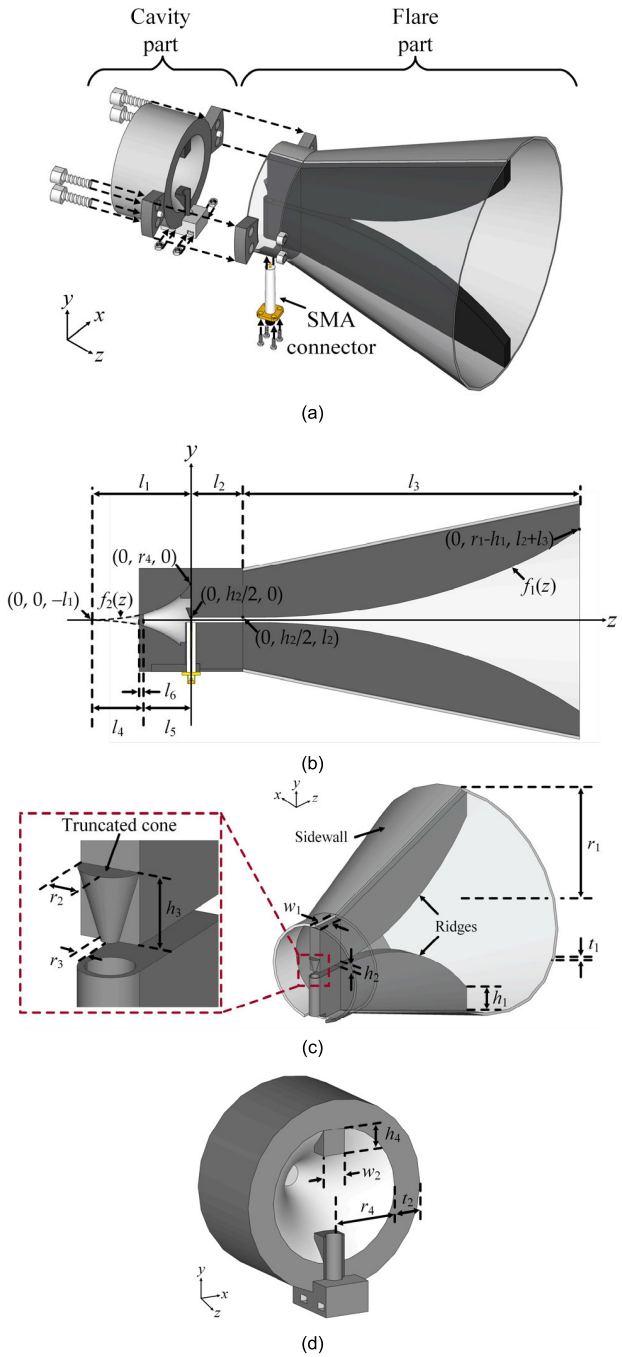

FIGURE 1. Geometry of the proposed antenna. (a) Isometric view. (b) Side view. (c) Flare part. (d) Cavity part.

aperture. In particular, horns with a ridge waveguide have been employed to extend the operating frequency range by shifting the cut-off frequency of the second propagation mode to a much higher frequency [14], [15], [16], [17], [18]. However, it is difficult to avoid an asymmetrical radiation pattern given the tilted main-lobe direction, and research to improve such radiation characteristics is required [19]. In addition, due to the sophisticated waveguide port and flare structure, there are disadvantages in manufacturing when using a conventional fabrication process. Recently, to resolve those issues,

TABLE 1. Design parameters of the proposed antenna.

Parameters	Optimized values
a_1	1.4
b_1	0.04
c_1	0.95
a_2	0.3
b_2	0.189
c_2	0.3
l_1	20 mm
l_2	10 mm
l_3	80 mm
l_4	10 mm
l_5	10 mm
l_6	1 mm
h_1	15 mm
h_2	0.9 mm
h_3	3.55 mm
h_4	8 mm
r_1	50 mm
r_2	2.75 mm
r_3	2 mm
r_4	13 mm
w_1	5.5 mm
w_2	9 mm
t_1	1 mm
t_2	11 mm

metal 3D printing technologies have been applied for such complicated horn fabrication [20], [21]. Even though the metal 3D printing is adopted, the horn antenna should be divided into several parts and then completed by assembling each separately fabricated part.

In this paper, we propose a double-ridged horn antenna with a truncated cone feeding structure, a curve-shaped cavity, and a mode suppressor to obtain symmetrical radiation patterns in a wide frequency range. To simplify both the manufacturing and assembly processes, the proposed antenna is designed to consist of only two parts (cavity and flare), which are fabricated using direct metal laser sintering (DMLS) 3D printing technology. In the flare part, a ridge is added to obtain the broadband characteristics, while a conducting sidewall is applied to decrease the half-power beamwidth (HPBW). At the starting position of the upper ridge, a truncated cone feeding structure is employed to obtain symmetrical radiation patterns in a wide frequency range. Moreover, the curve-shaped cavity is employed to improve the matching characteristics, and the mode suppressor inside the cavity is also applied to maintain stable bore-sight gain at a high frequency by suppressing the second-order mode [22]. The proposed antenna is fabricated and measured in a full

FIGURE 2. Photographs of the fabricated antenna. (a) Flare part. (b) Cavity part. (c) Proposed antenna (side view). (d) Proposed antenna (front view). (e) Measurement setup.

anechoic chamber to obtain its characteristics, such as reflection coefficients, gains, and radiation patterns. The performances of the antenna are compared with those of previous studies [23], [24], [25], [26]. The results demonstrate that the proposed antenna has broadband characteristics, stable boresight gain, and symmetrical radiation patterns, meaning that it is suitable for use as a feeder for SIGINT satellite reflector antenna.

II. DESIGN OF A DOUBLE-RIDGED HORN ANTENNA USING METAL 3D PRINTING

Fig. 1 shows the geometry of the proposed double-ridged horn antenna. This antenna consists of only two parts (cavity and flare), which are fabricated using metal 3D printing, and it is fed by an SMA connector, as shown in Fig. 1(a). Fig. 1(b) illustrates the cross-section (in the zy-plane) of the proposed antenna. The ridge and the cavity are designed with exponential functions based on equations (1) and (2), respectively, to achieve broadband characteristics. The ridge follows the function $f_1(z)$ in equation (1). Within the range of z from 0 to l_2, $f_1(z)$ has a constant value of $h_2/2$. After z exceeds l_2, it follows the exponential function starting at $(0, h_2/2, l_2)$ and ending at $(0, r_1\text{-}h_1, l_2+l_3)$, with a coefficient of a_1. By optimizing a_1, the curvature of the ridge enables a transition from 50 Ω impedance at the feeding point to 377 Ω impedance at the aperture of the horn antenna, extending

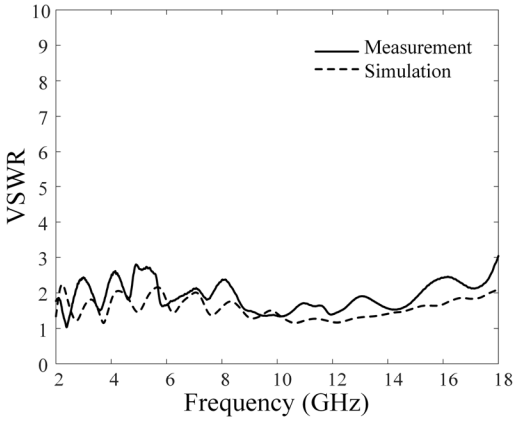

FIGURE 3. Measured and simulated VSWRs of the proposed antenna.

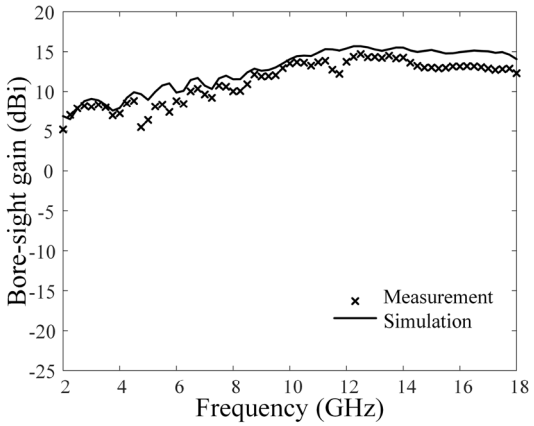

FIGURE 4. Measured and simulated bore-sight gains of the proposed antenna.

the frequency range of the fundamental mode [18]. With the aforementioned two points (start point $(0, h_2/2, l_2)$, end point $(0, r_1-h_1, l_2+l_3)$) and the optimized a_1, the values of b_1 and c_1 are decided correspondingly. Meanwhile, the curve-shaped cavity is designed to follow the exponential function $f_2(z)$ in equation (2), which connects two points, $(0, 0, -l_1)$ and $(0, r_4, 0)$, with the coefficient a_2. The a_2 is a critical parameter for achieving impedance matching at high frequencies, and it determines the values of b_2 and c_2. The cavity has a depth of l_5 to satisfy the matching characteristics in the operating frequency, as discussed in Chapter 3.

$$
\begin{aligned}
f_1(z) &= h_2/2, \quad (0 \le z < l_2) \\
f_1(z) &= a_1 \times e^{b_1(z-l_2)} - c_1, \quad (l_2 \le z < l_2 + l_3) \\
b_1 &= \ln(\frac{r_1 + c_1 - h_1}{a_1})/l_3, \quad c_1 = a_1 - h_2/2 \qquad (1) \\
f_2(z) &= a_2 \times e^{b_2(z+l_1)} - c_2, \\
b_2 &= \ln(\frac{r_4 + c_2}{a_2})/l_1, \quad c_2 = a_2 \qquad (2)
\end{aligned}
$$

Fig. 1(c) shows the flare part of the proposed antenna. The flare part consists of a conducting sidewall, ridge waveguide,

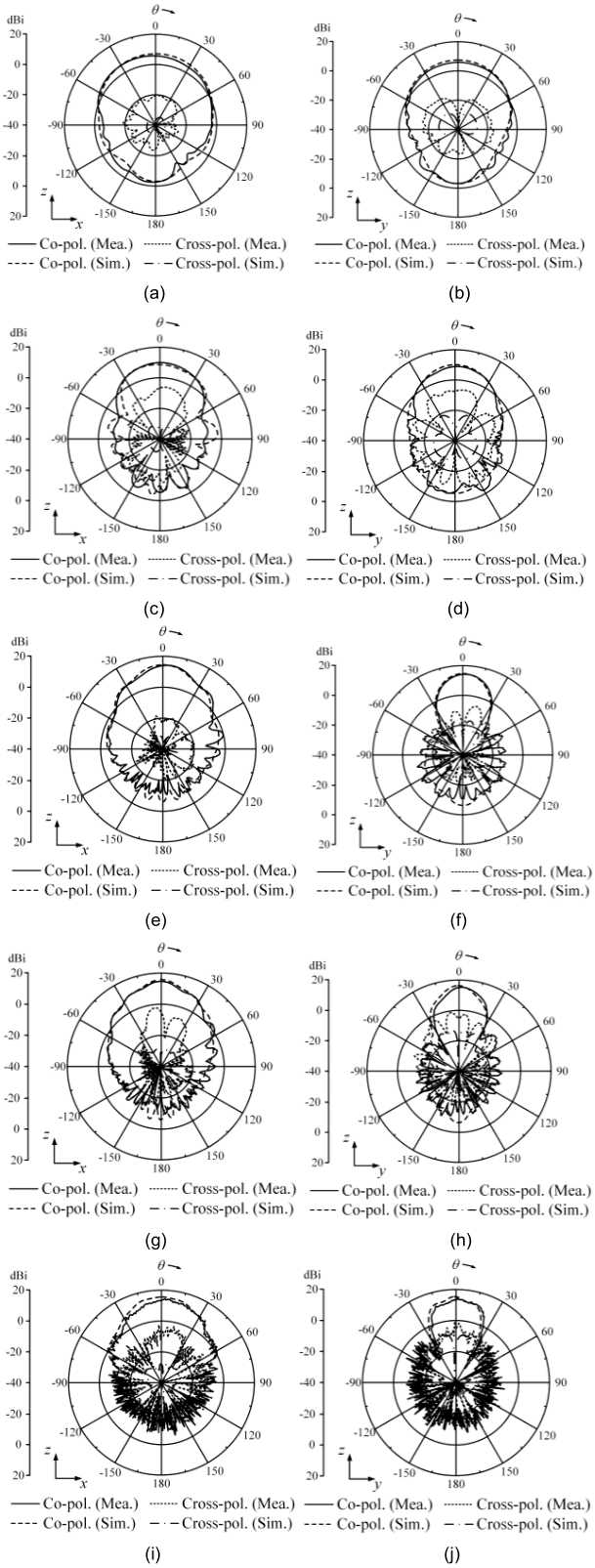

FIGURE 5. Measured and simulated radiation patterns of the proposed antenna. (a) zx-plane at 2 GHz. (b) zy-plane at 2 GHz. (c) zx-plane at 6 GHz. (d) zy-plane at 6 GHz. (e) zx-plane at 10 GHz. (f) zy-plane at 10 GHz. (g) zx-plane at 14 GHz. (h) zy-plane at 14 GHz. (i) zx-plane at 18 GHz. (j) zy-plane at 18 GHz.

TABLE 2. Comparisons between the proposed antenna and some previous studies.

Research	Band width (ratio)	Bore-sight gain at lowest Fre.	Bore-sight gain at highest Fre.	Size
[23]	8–18 GHz (2.25:1)	11.6 dBi	11.9 dBi	1.59 λ (60 mm) × 1.59 λ (60 mm) × 1.8 λ (68 mm)
[24]	6–18 GHz (3:1)	9.7 dBi	12.3 dBi	0.86 λ (42.8 mm) × 0.86 λ (42.8 mm) × 1 λ (50 mm)
[25]	2–6 GHz (3:1)	5 dBi	8 dBi	0.37 λ (56 mm) × 0.37 λ (56 mm) × 0.62 λ (93 mm)
[26]	6–20 GHz (3.3:1)	12 dBi	18 dBi	1.29 λ (64.5 mm) × 1.29 λ (64.5 mm) × 3.16 λ (158.43 mm)
This work	2–18 GHz (9:1)	5.37 dBi	14.5 dBi	0.66 λ (100 mm) × 0.66 λ (100 mm) × 0.67 λ (101 mm)

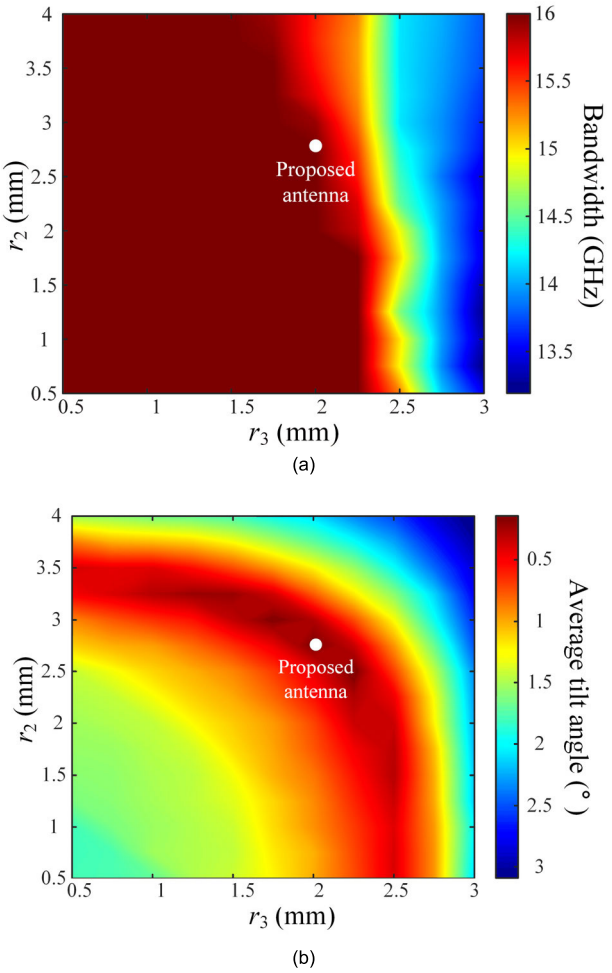

FIGURE 6. Bandwidth and average tilt angle of main-lobe direction in accordance with r_2 and r_3. (a) Bandwidth. (b) Average tilt angle.

and truncated cone feeding structure. The sidewall increases directivity by minimizing the electromagnetic field radiated to the sides and back, resulting in a decrease in the HPBW. This is important when designing the feeder of the reflector antenna because the radiated field from the feeder should be directed toward the reflector to achieve high spillover efficiency. When the beamwidth is too wide to extend beyond the reflector, the spillover efficiency of the reflector is reduced, and accordingly, the aperture efficiency is also reduced [9]. On the inner surface of this sidewall, the ridge waveguide is added to obtain broadband characteristics by shifting the cut-off frequency of the second propagation mode to a much higher frequency. The distance h_2 between the ridges at the feed point and the width of the ridge w_1 are the factors that determine the impedance. Since h_2 and w_1 affect the capacitance of the waveguide, these parameters are important in determining good impedance matching within the operating frequency band. In addition to the significance of these parameters for broadband, the feeding position between the ridge and the SMA connector is also a critical factor in improving matching characteristics. To that end, the inner conductor of the SMA connector should be connected to the start of the upper ridge. In order to connect the inner conductor to the start of the upper ridge, the lower ridge has to be slightly longer than the upper ridge. Due to the difference between the upper and lower ridges, asymmetrical currents are distributed, which causes the main-lobe direction to tilt. To solve this problem, the truncated cone (upper radius r_2, lower radius r_3, and height h_3) is employed at the start of the upper ridge. When the truncated cone is applied, a portion of the currents flows along the cone, which balances the currents between the ridges and reduces the tilt of the main-lobe direction. Fig. 1(d) presents the cavity part of the antenna, consisting of the curve-shaped cavity and the mode suppressor. It has a radius of r_4, a depth of l_5, and a wall thickness of t_2. The curvature of the curve-shaped cavity that improve matching characteristics is defined using equation (2). The mode suppressor, which is the conventional method to obtain stable bore-sight gains, is added inside the cavity. This has a height of h_4, a width of w_2, and is located between the

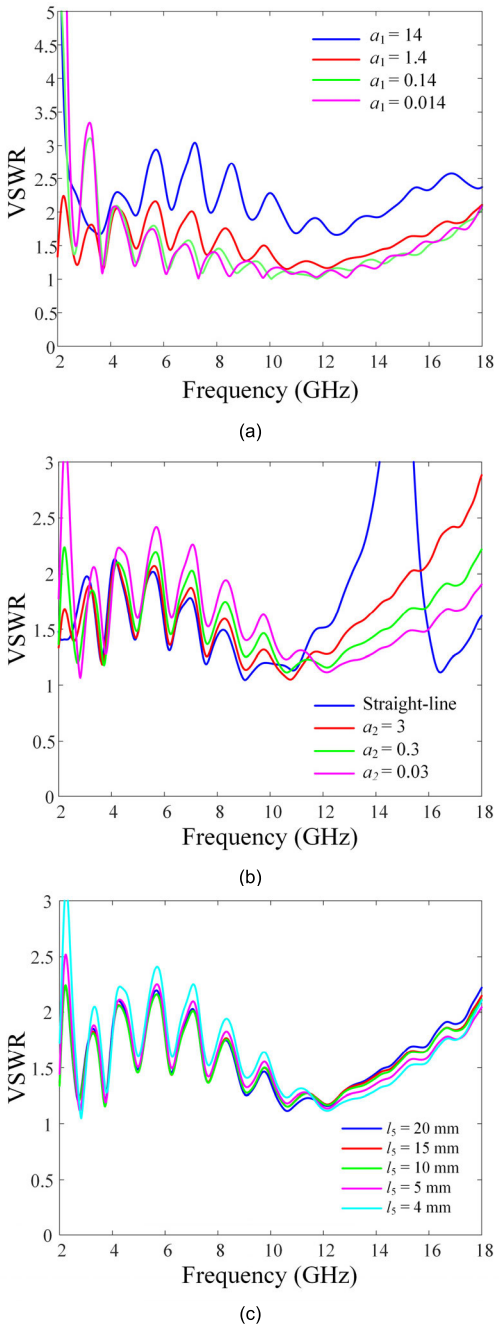

FIGURE 7. VSWRs in accordance with a_1, a_2 and l_5. (a) Depending on a_1 when $a_2 = 0.3$ and $l_5 = 20$ mm. (b) Depending on a_2 when $a_1 = 1.4$ and $l_5 = 20$ mm. (c) Depending on l_5 when $a_1 = 1.4$ and $a_2 = 0.3$.

curve-shaped cavity and the ridges. For frequencies above the cut-off of the second propagation mode, the currents flow toward the sidewall. These currents generate irregular fields, which result in the formation of a second-order pattern. However, the mode suppressor changes the currents distribution by redirecting the currents toward the cavity, preventing the second propagation mode. The proposed antenna is designed in the CST Studio Suite full EM simulator, and optimized design parameters are listed in Table 1 [27].

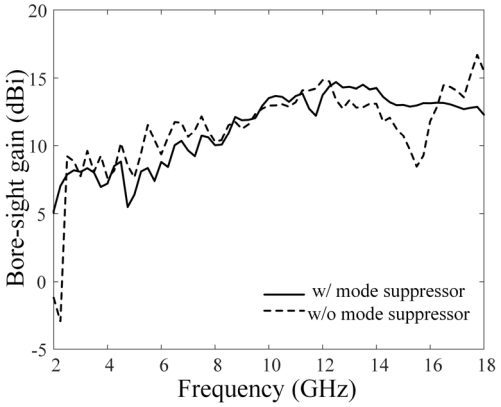

FIGURE 8. Measured bore-sight gains with and without the mode suppressor.

Fig. 2 represents photographs of the fabricated antenna. The proposed antenna consists of only two parts, which simplifies the manufacturing and assembly process. Each part is fabricated using the DMLS method with aluminum powders. DMLS is a 3D printing technology that melts and fuses multiple layers of metallic powders [28]. Fig. 2(a) shows the flare part of the antenna, which has the ridges, sidewall, and feeding structure. Two push pin holes are added for stable assembly. Fig. 2(b) illustrates the cavity part, consisting of the curve-shaped cavity and the mode suppressor. Two push pins are then combined with the push pin holes. As shown in Fig. 2(c), the flare part and the cavity part are assembled using bolts and nuts, and the SMA connector is also fastened using small bolts and nuts. This simplifies the assembly process and enables an electrical connection between the SMA connector and the antenna without soldering.

Fig. 3 shows the voltage standing wave ratios (VSWRs) of the proposed antenna, where solid and dashed lines indicate the measured and simulated results, respectively. The simulated VSWR has a maximum value of 2.2 and an average value of 1.6, while the measured VSWR has a maximum value of 3.0 and an average value of 1.9 in the range from 2 GHz to 18 GHz. Fig. 4 illustrates the bore-sight gains of the proposed antenna, where '×' marks and solid lines indicate the measured and simulated results. These results agree well, with an average difference of 1.95 dB. Fig. 5 presents the measured and simulated 2D radiation patterns (co- and cross-polarization) of the antenna in the zx- and zy-planes. Since the proposed antenna is designed to operate in linear polarization, the co-polarization patterns exhibit high gain characteristics, while the cross-polarization patterns show low gain characteristics, as shown in Figs. 5(a) to 5(j). For example, bore-sight gains for co-polarization in the zx-plane are 5.37 dBi by measurement and 6.76 dBi by simulation at 2 GHz. For cross-polarization, bore-sight gains are −20.7 dBi by measurement, and −37.8 dBi by simulation. The measured radiation patterns are in good agreement with the simulated results. Table 2 summarizes the comparisons between the proposed antenna and some previous studies.

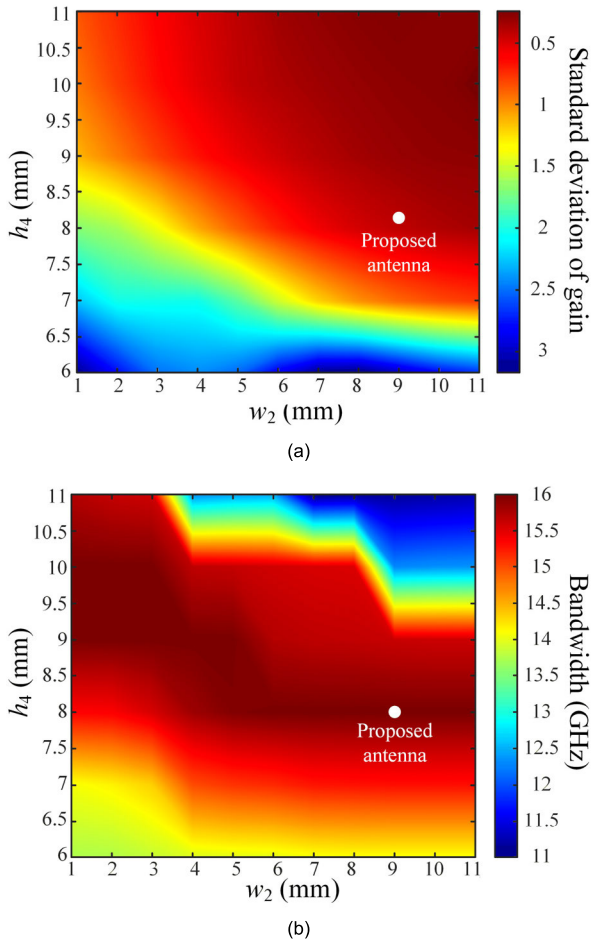

FIGURE 9. Standard deviation of gain and bandwidth in accordance with w_2 and h_4. (a) Standard deviation. (b) Bandwidth.

III. ANALYSIS

Fig. 6 illustrates the bandwidth (VSWR < 2.5) and the average main-lobe direction (E-plane) in accordance with the lower radius (r_3) and the upper radius (r_2) of the truncated cone. As shown in Fig. 6(a), when the value of r_3 is less than 1.5 mm, the bandwidth does not change significantly. When r_3 exceeds 1.5 mm, the bandwidth starts to decrease as r_3 increases. Meanwhile, there is no significant difference in bandwidth with changes to the value of r_2. Fig. 6(b) shows the average main-lobe direction by r_3 and r_2. The average tilt angle of the main-lobe direction is calculated by averaging from 2 GHz to 18 GHz in the zy-plane. To obtain a wide bandwidth and low average tilt angle, r_3 and r_2 are optimized to 2 mm and 2.75 mm, respectively. In the range from 2 GHz to 18 GHz, the obtained bandwidth is 16 GHz, and the average tilt angle is 0.15°, which is decreased by 1.6° compared to the result without the truncated cone.

Fig. 7(a) shows the VSWRs in accordance with the coefficient a_1 of function $f_1(z)$, which determines the curvature of ridges. When a_1 has a value of more than 1.4, VSWR becomes greater than 2.5 around 7 GHz and 16 GHz. On the other hand, when a_1 has a small value of less than 1.4, VSWR becomes greater than 2.5 in low frequency range below 4 GHz. To obtain the broadband characteristics ranging from 2 GHz to 18 GHz, the value of a_1 is determined to be 1.4. As shown in Fig. 7(b), the coefficient a_2 of function $f_2(z)$ also affects to the broadband characteristics. The curve-shaped cavity is designed by rotating the $f_2(z)$ around the z-axis. With a fixed cavity depth of l_5 (20 mm), the curvature of the cavity becomes a straight-line as a_2 increases, while the curvature of the cavity increases as a_2 decreases. The curvature of the cavity determines the matching characteristics for each frequency band. The value of a_2, which provides an optimal VSWR ranging from 2 GHz to 18 GHz, is determined to be 0.3. Fig. 7(c) demonstrates VSWRs in accordance with l_5. When l_5 is less than 10 mm, the matching characteristics are degraded at lower frequencies. Therefore, when considering the matching characteristics of the low frequency band, l_5 is determined to be 10 mm. When a_1 is 1.4, a_2 is 0.3, and l_5 is 10 mm, the bandwidth is 16 GHz, which is increased by 4.2 GHz compared with the straight-line cavity.

Fig. 8 shows the measured bore-sight gains with and without the mode suppressor. In the absence of the mode suppressor, currents that should flow on the ridge also flow toward the sidewall, resulting in unwanted high-order patterns. When the mode suppressor is applied, currents in the sidewall are redirected to the ridge, leading to a more stable bore-sight gain. Fig. 9(a) presents the standard deviation of the bore-sight gains from 12 GHz to 18 GHz, which illustrates their stability. This result shows that as both w_2 and h_4 increase, the standard deviation of gain decreases. However, as shown in Fig. 9(b), w_2 and h_4 with low standard deviation do not always result in a broad bandwidth. The optimized w_2 and h_4 are 9 mm and 8 mm, respectively, which gives a standard deviation of 0.43 and a bandwidth of 16 GHz. Compared to the case without the mode suppressor, the standard deviation is reduced by 3.78.

IV. CONCLUSION

We proposed the double-ridged horn antenna with the truncated cone feeding structure, curve-shaped cavity, and mode suppressor. The truncated cone feeding structure was employed to obtain symmetrical patterns and reduced the average tilt angle by 1.6°. The curve-shaped cavity was implemented to improve the matching characteristics, increasing the bandwidth by 4.2 GHz. Meanwhile, the mode suppressor was applied to maintain stable bore-sight gain, which reduced the standard deviation of gain by 3.78. The proposed antenna was designed to consist of only two parts and fabricated using metal 3D printing technology. The measured VSWR showed a maximum of 3.0 and an average of 1.9 from 2 GHz to 18 GHz. At 2 GHz, the measured bore-sight gains in the radiation pattern were 5.37 dBi for co-polarization and −20.7 dBi for cross-polarization. Through these results, it was confirmed that the proposed double-ridged horn antenna with broadband characteristics, stable bore-sight gains, and symmetrical patterns is suitable for use as a feeder for a reflector antenna.

REFERENCES

[1] S. Scalise, H. Ernst, and G. Harles, "Measurement and modeling of the land mobile satellite channel at Ku-band," *IEEE Trans. Veh. Technol.*, vol. 57, no. 2, pp. 693–703, Mar. 2008.
[2] J.-H. Lim, J. W. Lee, T.-K. Lee, S.-B. Ryu, H.-C. Lee, and S.-G. Lee, "Optimal design of the reflector antenna to improve performance of C-band quad-pol ScanSAR systems," *J. Electromagn. Eng. Sci.*, vol. 20, no. 2, pp. 155–157, Apr. 2020.
[3] S. Xue, X. Geng, L. Meng, T. Xie, L. Huang, and X.-H. Yan, "HISEA-1: The first C-band SAR miniaturized satellite for ocean and coastal observation," *Remote Sens.*, vol. 13, no. 11, p. 2076, May 2021.
[4] S. Wang, D. Jang, Y. Kim, and H. Choo, "Design of S/X-band dual-loop shared-aperture 2×2 array aperture," *J. Electromagn. Eng. Sci.*, vol. 22, pp. 319–325, May 2022.
[5] S.-I. Jeon, Y.-W. Kim, and D.-G. Oh, "A new active phased array antenna for mobile direct broadcasting satellite reception," *IEEE Trans. Broadcast.*, vol. 46, no. 1, pp. 34–40, Mar. 2000.
[6] J. Zhu, Y. Yang, Z. Hou, S. Liao, and Q. Xue, "Aperture-shared all-metal endfire high-gain parabolic antenna for millimeter-wave multibeam and sub-6-GHz communication applications," *IEEE Trans. Antennas Propag.*, vol. 71, no. 3, pp. 2784–2789, Mar. 2023.
[7] Z. A. Pour and L. Shafai, "Improved cross-polarization performance of a multi-phase-center parabolic reflector antenna," *IEEE Antennas Wireless Propag. Lett.*, vol. 13, pp. 540–543, 2014.
[8] S. Manafi, M. Al-Tarifi, and D. S. Filipovic, "45–110 GHz quad-ridge horn with stable gain and symmetric beam," *IEEE Trans. Antennas Propag.*, vol. 65, no. 9, pp. 4858–4863, Sep. 2017.
[9] W. L. Stutzman and G. A. Thiele, *Antenna Theory and Design*, 3rd ed. Hoboken, NJ, USA: Wiley, 2012.
[10] M. Pehlivan, K. Yegin, and Y. Asci, "Design of 1–18 GHz parabolic reflector antenna with LPDA feed," in *Proc. 24th Telecommun. Forum (TELFOR)*, Nov. 2016, pp. 1–3.
[11] Y. Rahmat-Samii and S.-W. Lee, "Directivity of planar array feeds for satellite reflector applications," *IEEE Trans. Antennas Propag.*, vol. AP-31, no. 3, pp. 463–470, May 1983.
[12] K.-H. Lee, C.-C. Chen, and R. Lee, "UWB dual-linear polarization dielectric horn antennas as reflector feeds," *IEEE Trans. Antennas Propag.*, vol. 55, no. 3, pp. 798–804, Mar. 2007.
[13] C. Yu, W. Hong, L. Chiu, G. Zhai, C. Yu, W. Qin, and Z. Kuai, "Ultrawideband printed log-periodic dipole antenna with multiple notched bands," *IEEE Trans. Antennas Propag.*, vol. 59, no. 3, pp. 725–732, Mar. 2011.
[14] J. S. Kim, H. S. Park, Y. J. Yoon, J. Ryu, and J. S. Choi, "Modified TEM horn for enhanced radiation characteristics at low frequency," *J. Electromagn. Eng. Sci.*, vol. 14, no. 2, pp. 74–78, Jun. 2014.
[15] A. Akgiray, S. Weinreb, W. A. Imbriale, and C. Beaudoin, "Circular quadruple-ridged flared horn achieving near-constant beamwidth over multioctave bandwidth: Design and measurements," *IEEE Trans. Antennas Propag.*, vol. 61, no. 3, pp. 1099–1108, Mar. 2013.
[16] B. Jacobs, J. W. Odendaal, and J. Joubert, "Compact 0.5–18 GHz double-ridged guide horn antenna," *IET Microw., Antennas Propag.*, vol. 15, no. 4, pp. 427–440, Mar. 2021.
[17] S. Hopfer, "The design of ridged waveguides," *IEEE Trans. Microw. Theory Techn.*, vol. MTT-3, no. 5, pp. 20–29, Oct. 1955.
[18] K. L. Walton and V. C. Sundberg, "Broadband ridged horn design," *Microw. J.*, vol. 4, no. 2, pp. 96–101, Mar. 1964.
[19] S. Bruns, P. Leuchtmann, and R. Vahldieck, "Analysis and simulation of a 1–18-GHz broadband double-ridged horn antenna," *IEEE Trans. Electromagn. Compat.*, vol. 45, no. 1, pp. 55–60, Feb. 2003.
[20] F. Oktafiani, E. Y. Hamid, and A. Munir, "Wideband dual-polarized 3D printed quad-ridged horn antenna," *IEEE Access*, vol. 10, pp. 8036–8048, 2022.
[21] M. A. Al-Tarifi and D. S. Filipovic, "On the design and fabrication of W-band stabilised-pattern dual-polarised horn antennas with DMLS and CNC," *IET Microw., Antennas Propag.*, vol. 11, no. 14, pp. 1930–1935, Sep. 2017.
[22] Y. Ma, C. H. See, F. Pang, D. Wu, D. Liu, Z. Z. Abidin, S. Keates, B. Peng, and R. A. Abd-Alhameed, "A 10:1 bandwidth cryogenic quadruple-ridged flared horn design for reflector antennas in radio astronomy," *IEEE Access*, vol. 8, pp. 81101–81115, 2020.
[23] V. Rudakov, V. Sledkov, and M. Manuilov, "Compact over-octave horn antenna with stable radiation pattern," in *Proc. IEEE 8th All-Russian Microw. Conf. (RMC)*, Nov. 2022, pp. 140–143.
[24] A. Kazerooni and A. Dastranj, "Design and experiment of a conical double-ridged horn antenna for 6–18 GHz," *Int. J. RF Microw. Comput.-Aided Eng.*, vol. 21, no. 3, pp. 336–342, Mar. 2011.
[25] S. Sarjoghian, M. H. Sagor, Y. Alfadhl, and X. Chen, "A 3D-printed high-dielectric filled elliptical double-ridged horn antenna for biomedical monitoring applications," *IEEE Access*, vol. 7, pp. 94977–94985, 2019.
[26] S. Manshari, S. Koziel, and L. Leifsson, "A wideband corrugated ridged horn antenna with enhanced gain and stable phase center for X- and Ku-band applications," *IEEE Antennas Wireless Propag. Lett.*, vol. 18, no. 5, pp. 1031–1035, May 2019.
[27] (2023). *CST Studio Suite: Electromagnetic Field Simulation Software*. [Online]. Available: http://www.cst.com
[28] M. Shellabear and O. Nyrhilä, "DMLS-development history and state of the art," in *Proc. LANE*, Erlangen, Germany, Sep. 2004, pp. 21–24.

NAMKANG LEE received the B.S. degree in electronic and electrical engineering from Hongik University, Seoul, South Korea, in 2023. His research interests include system on chip, ultra-wideband communications, microwave systems, and satellite communications.

CHANGHYEON IM received the B.S. degree in electronic and electrical engineering from Hongik University, Seoul, South Korea, in 2021, where he is currently pursuing the Ph.D. degree in electronic and electrical engineering. His research interests include mesh reflector antenna, 5G application, wireless power transfer, and ultra-wideband antenna.

SEULGI PARK received the B.S. and M.S. degrees in electrical engineering from Hongik University, in 2006 and 2008, respectively. He was with the Electronic Warfare Research Center, LIG Nex1 Corporation, from 2008 to 2013, and DMC Research Center, Samsung Electronics Corporation, from 2013 to 2016. Since January 2017, he has been with the Tactical Communication System Team, Hanwha Systems. His major research interests include electronic warfare transmission/reception antennas, electronic warfare systems, and tactical communication systems.

HOSUNG CHOO (Senior Member, IEEE) received the B.S. degree in radio science and engineering from Hanyang University, Seoul, South Korea, in 1998, and the M.S. and Ph.D. degrees in electrical and computer engineering from The University of Texas at Austin, in 2000 and 2003, respectively. In September 2003, he joined the School of Electronic and Electrical Engineering, Hongik University, Seoul, where he is currently a Professor. His research interests include electrically small antennas for wireless communications, reader and tag antenna for RFID, on-glass and conformal antennas for vehicles and aircraft, and array antenna for GPS applications.